

# Molecular Dynamics Simulation of the Salinity Effect on the *n*-Decane/Water/Vapor Interfacial Equilibrium

Jin Zhao,<sup>†</sup><sup>ID</sup> Guice Yao,<sup>†</sup> Srinivasa B. Ramisetty,<sup>†</sup> Robert B. Hammond,<sup>†</sup> and Dongsheng Wen<sup>\*,‡,†</sup><sup>ID</sup>

<sup>†</sup>School of Chemical and Process Engineering, University of Leeds, Leeds LS2 9JT, United Kingdom

<sup>‡</sup>School of Aeronautic Science and Engineering, Beihang University, Beijing 100191, People's Republic of China

**ABSTRACT:** Low-salinity water flooding of formation water in rock cores is, potentially, a promising technique for enhanced oil recovery (EOR), but details of the underlying mechanisms remain unclear. The salinity effect on the interface between water and oil was investigated here using the molecular dynamics (MD) simulation method. *n*-Decane was selected as a representative oil component, and SPC/E water and all-atom optimized potentials for liquid simulations (OPLS-AA) force fields were used to describe the water/oil/ionic interactions for saltwater and *n*-decane molecules. Equilibrium MD simulations were first conducted to study the *n*-decane/vapor and saltwater/vapor interface systems at six different NaCl concentrations (0, 0.05, 0.10, 0.20, 0.50, and 1.00 M). The water/oil interface was then investigated by calculating bulk density distribution, radial distribution function, interface thickness, and water/oil interfacial tension (IFT). Sufficiently long MD simulations of water/*n*-decane/vapor were performed, followed by an analysis of the effect of salinity on the water/oil/vapor interface. The IFT values for the water/vacuum interface, *n*-decane/vacuum interface, and water/*n*-decane interface were obtained from the pressure tensor distribution after system equilibration, with values of 71.4, 20.5, and 65.3 mN/m, respectively, which agree well with experimental and numerical results reported in the literature. An optimal salinity of ~0.20 M was identified corresponding to a maximum interfacial thickness between water and the oil phase, which results in a minimum water/oil IFT value and a maximum value for the oil/water contact angle, a condition beneficial for EOR.

## 1. INTRODUCTION

Enhanced oil recovery (EOR) is becoming more and more important to maximize recovery from existing oil fields to meet the increasing global energy demand and mitigate environmental impact.<sup>1</sup> Low-salinity flooding, i.e., injecting lower salinity water (usually specified as having a 1:1 electrolyte concentration of less than about 5000 ppm) into formation water, has been of interest as an EOR technique<sup>2</sup> since the publication of the first experimental evidence by Jadhunandan and Morrow.<sup>3</sup> It was soon found that an enhancement is not observed consistently but is dependent upon a number of factors, including connate water saturation, the salinity of connate water, injection water salinity, and wettability.<sup>4</sup> No less than 17 recovery mechanisms behind the low-salinity EOR process have been proposed in the literature, but many of them are related to one another.<sup>5</sup> As a result of the complexities of oil components and reservoir rock formations, the recovery mechanisms underpinning the low-salinity EOR process are still unclear. Two physical properties that, when manipulated, are influential on low-salinity EOR phenomena are substrate wettability and the interfacial tension (IFT) between the oil and brine (when reduced).<sup>6</sup> The interfaces between immiscible liquids are therefore fundamental in understanding EOR mechanisms. Interfaces are, by definition, discontinuities in nature, but it must also be recognized that there is a fundamental difference between a single interface considered in isolation, e.g., between two immiscible liquid components in the bulk, and two or more interfaces in very close proximity, for example, having two solid surfaces separated by a thin liquid layer comprised of two immiscible liquid components, such as an aqueous electrolyte and a hydrocarbon.

The IFT between oil and water is one of the key properties determining the mobility of trapped oil in reservoir rocks.<sup>7–10</sup> Experimentally, the effect of salts on IFT and, consequently, on oil recovery efficiency has been investigated for several decades but with contradictory results. For instance, Aveyard et al.<sup>11</sup> first reported that the IFT increased linearly for the dodecane–water system as the molality of the electrolyte of different kinds is increased, except in the case of potassium iodide, which showed a decreasing trend. Later, Ikeda et al.<sup>12</sup> measured the IFT of water/hexane as a function of the sodium chloride concentration using the pendant drop method and showed an increase of IFT when increasing the salt concentration from 0 to 1 M, which is consistent with results from Badakshan et al.<sup>13</sup> and Cai et al.<sup>14</sup> In contrast, Serrano et al.<sup>15</sup> observed fluctuations in IFT values for oil/brine at different salt concentrations, and Alotaibi et al.<sup>16</sup> indicated that low salinity did not always reduce the IFT of water/*n*-dodecane. After equilibrium was reached at 5 min of elapsed time, the IFT of the 5 wt % NaCl solution decreased in contrast with two other concentrations of 2 and 10 wt %.<sup>16</sup> The exact causes of such contradictory observations regarding the effect of salts on IFT remain unclear and require fundamental insights at the molecular level. To this end, a few experimental studies at the molecular scale have been carried out at liquid/solid interfaces, e.g., by X-ray crystallography, to understand the properties of water molecules located next to hydrophobic surfaces, including the orientation of water molecules and their

Received: March 1, 2018

Revised: September 17, 2018

Published: September 18, 2018



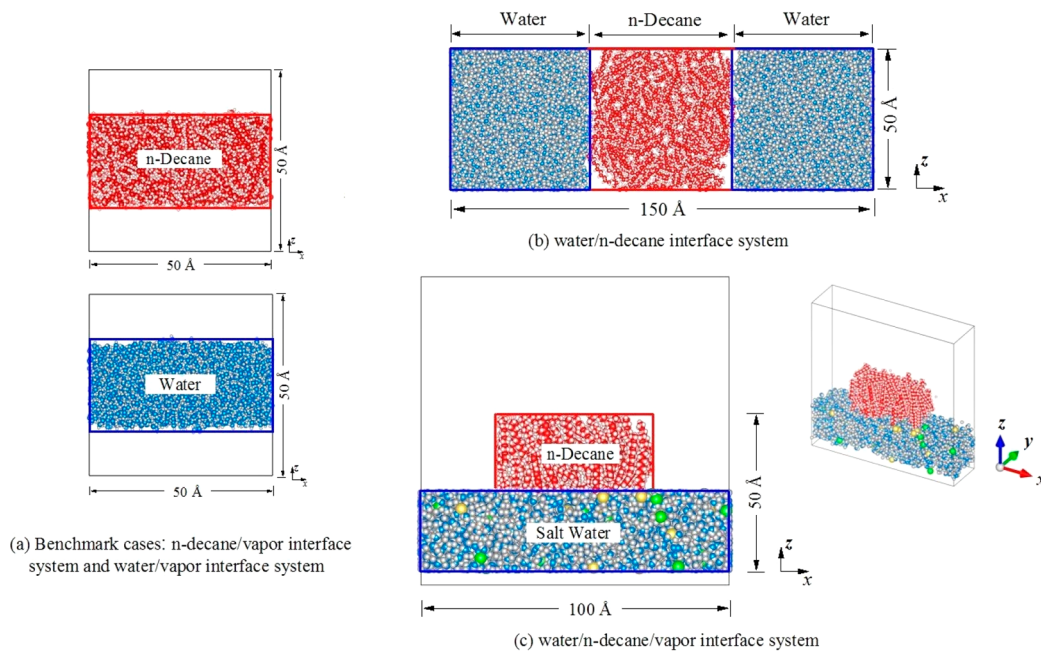


**Figure 1.** Initial configurations of the simulation systems.

hydrogen-bonding interactions.<sup>17,18</sup> However, experimental measurements for liquid–liquid interfaces at nanoscale are still very difficult to achieve because such interfaces are diffuse in comparison to solid/liquid interfaces. Consequently, experimental measurements at liquid/liquid interfaces are often associated with large uncertainties, and the detection of the influence of structural properties of oil at the interface is challenging.

Whereas a suitable continuum model may be sufficient to model the interface between water and oil components in the bulk and its sensitivity to the aqueous electrolyte concentration, an atomistic modeling approach can yield significant insights into the effect of a reduction in the smallest length-scale, which defines the separation distance between two solid surfaces when modeling a pore in an oil–reservoir rock. An appropriate atomistic approach to explore effects associated with confinement and small length scales is classical molecular dynamics (MD), which has been recently adopted to provide fundamental information on the molecular interactions and fluid flow at nanoscale. A few MD studies have been conducted for EOR applications,<sup>19,20</sup> including the prediction of thermophysical properties, such as viscosity and thermal conductivity.<sup>21–23</sup> On the interfacial properties, Jungwirth et al.<sup>24</sup> investigated the effect of inorganic ions on the air/water interface by MD simulation and found that the simulation results were consistent with experimental evidence. D'Auria et al.<sup>25,26</sup> carried out both dissipative particle dynamics (DPD) and classical MD simulations of aqueous solutions of sodium chloride at two different concentrations using polarizable and standard additive force fields, showing that the presence of chloride ions at the air–solution interface is reconcilable with the classical thermodynamic results of the Gibbs absorption theory. Sun et al.<sup>27</sup> investigated the surface tension and structure of salt solutions and clusters and showed that the van der Waals interactions had a large impact on the distribution of the halide anions and that conventional force field parameters needed to be optimized to increase the accuracy of IFT prediction. Buuren et al.<sup>28</sup> performed MD simulations on the

sensitivity of surface properties to the van der Waals parameters for the decane/water interface, followed by Zeppieri et al.,<sup>29</sup> Jang et al.,<sup>30</sup> and Mitrinović et al.<sup>31</sup> Kunieda et al.<sup>32,33</sup> investigated the spreading of multicomponent oils on water with MD simulations and predicted the IFTs between water and oil mixture components, including decane, toluene, and heptane. Zhang et al.<sup>34</sup> investigated the structural and dynamical properties of the NaCl solution/n-decane interface and found that NaCl salts caused an increase in the surface tension but did not affect the molecular orientation significantly. These studies showed that, properly used, MD could provide fundamental information, inaccessible via experimental measurements, into the structure properties of interfacial systems. The current MD studies, however, have been exclusively focused on two-phase equilibrium between water and a single oil component, and the presence of substrate and the vapor phase, which could have significant influence on the interfacial properties, has not been considered explicitly.

Four interface systems were investigated by MD simulations in this paper, namely, *n*-decane/vapor interface, water/vapor interface, saltwater/*n*-decane interface, and saltwater/*n*-decane/vapor interface systems. The purpose of this contribution is 2-fold: first to demonstrate the suitability of the choice of interatomic force field and calculation setup by applying MD to model the bulk interface between vapor and liquid phases (water containing varying concentrations of sodium chloride and *n*-decane) and second to apply the approach to the more complex cases of the saltwater/*n*-decane interface and saltwater/*n*-decane/vapor interface systems. The influences of aqueous NaCl solutions at six different concentrations from 0.00 [deionized (DI) water] to 1.00 M were examined to investigate salinity effects at the interface. The radial distribution function (RDF), density distributions, interface thickness, contact angle, and IFT of the species were calculated and analyzed in each system to reveal the fundamental influence of salts for low-salinity EOR application.

## 2. METHODOLOGY

The details about model construction are presented in this section. The MD simulation technique is described along with details of how the molecular pressure tensors, density profiles, IFT, and interfacial thickness were extracted from the simulation trajectory files.

**2.1. Model Construction.** To investigate the salinity effect on the water/oil/vapor interfacial equilibrium, *n*-decane ( $C_{10}H_{22}$ ) molecules were considered as representative of the oil phase. Decane is a typical component of petroleum and has been presented frequently in the literature as a kerosene surrogate or as the main component of diesel surrogates. Aqueous NaCl solutions were selected as a representative 1:1 electrolyte with six different salt concentrations, which were 0.00 (DI water), 0.05, 0.10, 0.20, 0.50, and 1.00 M.

Figure 1 shows the simulation procedure and the initial configurations of systems: (a) The validation of our simulations is first demonstrated by a careful benchmark of the approach on smaller systems representing *n*-decane/vapor and saltwater/vapor interfaces. In section 3.1, both the *n*-decane/vapor interface system and saltwater/vapor system were constructed by building one *n*-decane or water slab in the middle of a cubic box with two vapor spaces on either side. (b) To investigate the saltwater/*n*-decane interface in section 3.2, two rectangular aqueous electrolyte blocks were built, separated by a distance of 4.0 Å, and the intervening volume element was filled with randomly orientated *n*-decane molecules. (c) For the saltwater/*n*-decane/vapor interface system reported in section 3.3, a three-phase system was established to visualize the contact angle directly by initially inserting an *n*-decane droplet onto a water slab, with a separation distance of 4.0 Å. It is notable that this saltwater/*n*-decane/vapor three-phase system was made as an apparent two-dimensional system. The advantages of such an approach compared to a fully three-dimensional (3D) model are as follows: (i) computational time can be saved because a small length in the depth direction can be taken, and (ii) effects caused by the droplet size on the contact angle can be ignored because the radius of curvature is infinity on the straight three-phase contact line. The PACKMOL<sup>35</sup> package was used to construct all of the initial configurations for the simulations with both water and *n*-decane molecules randomly distributed and orientated in the simulation box initially.

To remove any high strain for the initial configurations, energy minimization was performed using the steepest descent method before the equilibrium MD simulations were carried out. Periodical boundary conditions were used in all systems with different spatial dimensions, as shown in panels a–c of Figure 1, with a total density of 1.00 g/cm<sup>3</sup> for the water phase and 0.73 g/cm<sup>3</sup> for the oil phase.

**2.2. Force Fields.** In these simulations, *n*-decane interactions were described using the all-atom optimized potentials for liquid simulations (OPLS-AA) force field<sup>21</sup> and the SPC/E force field was used for water.<sup>22</sup> The sodium and chloride ions were modeled as charged Lennard-Jones particles<sup>36</sup> using the parametrizations of the OPLS-AA force field. These force fields were tested extensively and successfully used in previous simulations.<sup>8,37–39</sup> The total energy is given by eq 1, including both the intra- and intermolecular interactions

$$E_{\text{total}} = E_{\text{bond}} + E_{\text{angle}} + E_{\text{dihedral}} + E_{\text{torsion}} + E_{\text{vdw}} + E_{\text{Coulombic}} \quad (1)$$

where  $E_{\text{total}}$ ,  $E_{\text{bond}}$ ,  $E_{\text{angle}}$ ,  $E_{\text{dihedral}}$ ,  $E_{\text{torsion}}$ ,  $E_{\text{vdw}}$ , and  $E_{\text{Coulombic}}$  are the total energy, bond-stretching, angle-bending, dihedral energy, torsion energy, van der Waals, and electrostatic components, respectively. The Lennard-Jones potential parameters ( $\epsilon_{ij}$  and  $\sigma_{ij}$ ) between different atom types were obtained using geometric combining rules, as shown in eqs 2 and 3.

$$\sigma_{ij} = \sqrt{\sigma_{ii}\sigma_{jj}} \quad (2)$$

$$\epsilon_{ij} = \sqrt{\epsilon_{ii}\epsilon_{jj}} \quad (3)$$

In the simulations, all of the atoms were free to adjust their positions to attain equilibrium structures.

**2.3. Equilibrium MD Simulation Details.** All equilibrium MD calculations were performed using the DL\_POLY molecular simulation package.<sup>40</sup> The Leapfrog integration algorithm was used with a time step of 1.0 fs in all simulations. The potential energy was evaluated with a 10.0 Å cutoff distance for the short-range van der Waals interaction, and a comparison to further simulations using a larger cutoff distance of 12.0 Å was conducted to check that the simulations employing a 10.0 Å cutoff were energy-converged. The Ewald summation for the Columbic interactions (smoothed particle mesh Ewald in DL\_POLY) was calculated with a precision of  $1 \times 10^{-6}$ . A Berendsen thermostat with a relaxation time of 0.1 ps was used to control the system temperature. To remove initial strain, energy minimization (steepest descent) was performed on the initial configuration for  $1 \times 10^4$  steps. The MD simulation was subsequently started in the NPT ensemble with an equilibration period of 50 ps at 0.10 MPa and with initial velocities taken for a Maxwellian distribution at 300 K, meanwhile coupling the system to an external heat bath at 300 K with a constant time step of 0.001 ps. After equilibration, the volume of the system was then kept fixed and another 5 ns of NVT ensemble simulation was conducted with all covalent bond lengths as well as the water bond angle constrained by the procedure SHAKE (tolerance of  $1 \times 10^{-5}$  nm).

**2.4. Calculation Methods.** Here, the pressure tensor for the interface system was obtained using the virial equation (eq 4)

$$P_{\alpha\beta} = \frac{1}{V} \left( \sum_{i=1}^N m_i v_{i\alpha} v_{i\beta} + \sum_{i=1}^{N-1} \sum_{j=i+1}^N F_{ija} r_{ij\beta} \right) \quad (4)$$

where  $P_{\alpha\beta}$  is an element in the pressure tensor,  $\alpha$  and  $\beta$  are the directional components,  $V$  is the volume,  $m_i$  is the mass of particle  $i$ ,  $v_{i\alpha}$  is its velocity in the  $\alpha$  direction,  $F_{ija}$  is the  $\alpha$  component of the total force on particle  $i$  as a result of particle  $j$ , and  $r_{ij\beta}$  is the  $\beta$  component of the vector ( $r_i - r_j$ ). The kinetic contribution to the pressure is given by the first term in this equation, and the virial contribution is given by the second term in this equation. The three diagonal elements in the pressure tensor represent the relevant pressure components.

The IFT  $\gamma$  of the saltwater/*n*-decane interface normal to the  $z$  axis can be calculated from the pressure tensor distribution after equilibration using the mechanical definition<sup>41,42</sup> as eq 5

$$\gamma = - \int (p'(z) - p) dz \quad (5)$$

where  $p'(z)$  is the lateral pressure,  $p$  is the bulk pressure, and the integral is defined over the boundary layer. With two interfaces perpendicular to the  $z$  axis, this gives the following relationship (eq 6) for the IFT

$$\gamma = -\frac{1}{2} \left( \frac{p_x + p_y}{2} - p_z \right) L_z \quad (6)$$

in which  $p_\alpha = P_{\alpha\alpha}$  ( $\alpha = x, y, z$ ) and  $L_z$  is the box length in the  $z$  direction used for the calculation. For the three-phase water/*n*-decane/vapor systems, by assuming that the local interfaces far from the three-phase contact line are parallel to the  $xy$  plane, the local pressure distributions were used over the range of  $40 \leq x \leq 60$  and  $20 \leq y \leq 60$  Å when calculating the water/decane IFT, which can be expressed as

$$\gamma = - \left( \frac{p_x + p_y}{2} - p_z \right) L_z \quad (7)$$

The planar density profiles for the simulations can be used to describe the probability of finding an atom within a planar element  $df_c$  along a Cartesian axis using eq 8

$$\rho(f_c) = n_f / N df_c \quad (8)$$

where the value  $N$  is the number of total atoms and  $n_f$  is the number of atoms within a planar element  $df_c$ .

To characterize the thickness of the vapor/liquid interface in the simulations, the “10–90” interfacial thicknesses,  $t$ , are obtained by

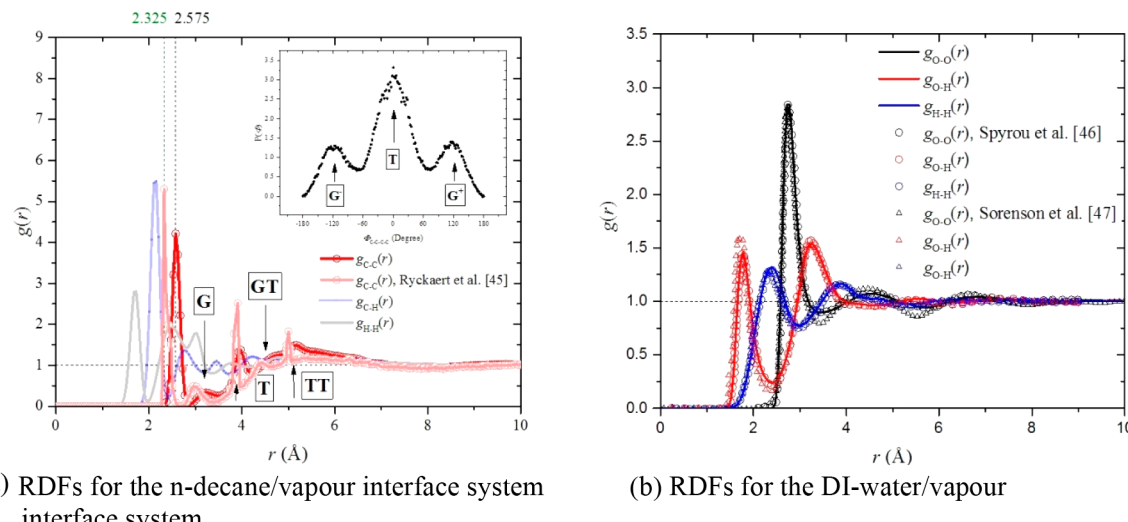


**Figure 2.** RDF profiles for the *n*-decane/vapor interface and DI water/vapor interface systems.<sup>45–47</sup>

fitting each of the two equilibrium molecular density profiles,  $\rho(z)$ , to a hyperbolic tangent function of the form given in eq 9<sup>43</sup>

$$\rho(z) = \frac{1}{2}(\rho_L + \rho_V) - \frac{1}{2}(\rho_L - \rho_V)\tanh\left(\frac{z - z_0}{t}\right) \quad (9)$$

where  $\rho_L$  and  $\rho_V$  are the liquid and vapor densities, respectively,  $z_0$  is the location of the Gibbs dividing surface, and the interface thickness  $t$  is calculated as the distance between two positions where the density varies from 10 to 90% of the density of the bulk phase. As a result, this thickness is known as the “10–90” interfacial thickness. A frequently used alternative thickness is the “10–50” interfacial thickness, which is defined analogously. To be more specific, the “10–90” interfacial thickness criterion was adopted by defining the interfacial thickness to be the distance along the interface over which the density changes from a value of 10–90% of the total density change between the bulk, i.e., the spatial extent over which the density varies from  $\rho_{VB} + 0.1(\rho_{LB} - \rho_{VB})$  to  $\rho_{VB} + 0.9(\rho_{LB} - \rho_{VB})$ , where  $\rho_{VB}$  and  $\rho_{LB}$  are the vapor and liquid bulk densities, respectively.

For systems exhibiting liquid–liquid equilibrium, the thickness of the water/*n*-decane interface was calculated using the criteria proposed by Senapati and Berkowitz.<sup>44</sup> The density profile of each component is fitted to an error function form given by eqs 10 and 11

$$\rho_W(z) = \frac{1}{2}\rho_{WB} - \frac{1}{2}\rho_{WB} \operatorname{erf}\left[\frac{z - z_W}{\sqrt{2}t_C}\right] \quad (10)$$

$$\rho_D(z) = \frac{1}{2}\rho_{DB} + \frac{1}{2}\rho_{DB} \operatorname{erf}\left[\frac{z - z_D}{\sqrt{2}t_C}\right] \quad (11)$$

where  $\rho_W(z)$  and  $\rho_D(z)$  are the density profiles of water and decane, respectively,  $\rho_{WB}$  and  $\rho_{DB}$  are the water and decane bulk densities, respectively,  $\langle z_W \rangle$  and  $\langle z_D \rangle$  are the average positions of the individual Gibbs dividing surfaces for each interface, and erf is the error function. The contribution from the intrinsic width to the interfacial thickness  $t_0$  is determined from the difference between the positions of the fitted interfaces as  $t_0 = |\langle z_D \rangle - \langle z_W \rangle|$ , and the contribution of thermal fluctuations to the interfacial width is determined by the value of the “10–50” interfacial thickness  $t_C$ . The total interfacial width is then given by eq 12.

$$t^2 = t_0^2 + t_C^2 \quad (12)$$

### 3. RESULTS AND DISCUSSION

Section 3.1 discusses the validity of the choice of interatomic force field and calculation setup through applying MD to

model two validation cases (*n*-decane/vapor and saltwater/vapor interfacial equilibrium systems). Sections 3.2 and 3.3 report the salinity effect on the saltwater/decane interface and saltwater/decane/vapor interface at six electrolyte concentrations.

**3.1. Benchmark Cases for Validation: (a) *n*-Decane/Vapor Interfacial Equilibrium and (b) Effects of Salinity on the Saltwater/Vapor Interfacial Equilibrium Simulations.** The validation of our simulations is demonstrated by a careful benchmarking of the approach on simpler systems, namely, *n*-decane/vapor and saltwater/vapor interfaces, as reported in this section. After 5 ns of simulation time for both systems, the energy, pressures, and temperatures of all components were considered to be equilibrated. This was checked in one case by extending the simulation time by a further 3 ns with no significant changes observed in the relevant parameter values. It should be noted that the calculated densities of the *n*-decane phase in the *n*-decane/vapor system ( $0.728 \pm 0.063$ ) and water phase in each saltwater/vapor system ( $0.998 \pm 0.027$ ) agree well with those of the pure bulk phases ( $0.73 \text{ g/cm}^3$  for *n*-decane and  $1.00 \text{ g/cm}^3$  for water). This shows that the simulations are sufficiently long for studying a realistic interface between two bulk phases.

The RDF of molecules in both *n*-decane/vapor and DI water/vapor interface systems were sampled, as shown in Figure 2: (1) The interaction between two *n*-decane molecules can be seen from the RDF profiles in Figure 2a, where intra- and intermolecular correlations are mixed. As far as the intermolecular correlations are concerned, it is clear that the oscillations around  $g(r) = 1$  are close to the cutoff radius. *Trans* (T) and *gauche* (G) conformation positions of carbon atom neighbors in a molecule can also be observed, followed with successive GT and TT conformations, as marked in Figure 2a. To characterize the conformations of *n*-decane molecules in the *n*-decane/vapor interface system, the probability density function (PDF) distribution for the *n*-decane molecules as a function of the internal dihedral angle  $\Phi_{C-C-C-C}$  was calculated, as shown in Figure 2a, where the peaks observed at  $\Phi_{C-C-C-C} = 0^\circ$  and  $\Phi_{C-C-C-C} = \pm 120^\circ$  correspond respectively to *trans* (T) and *gauche* ( $G^+$  and  $G^-$ ) conformations. The magnitudes of the  $G^+$  and  $G^-$  peaks are very close, corresponding to the symmetry of the dihedral

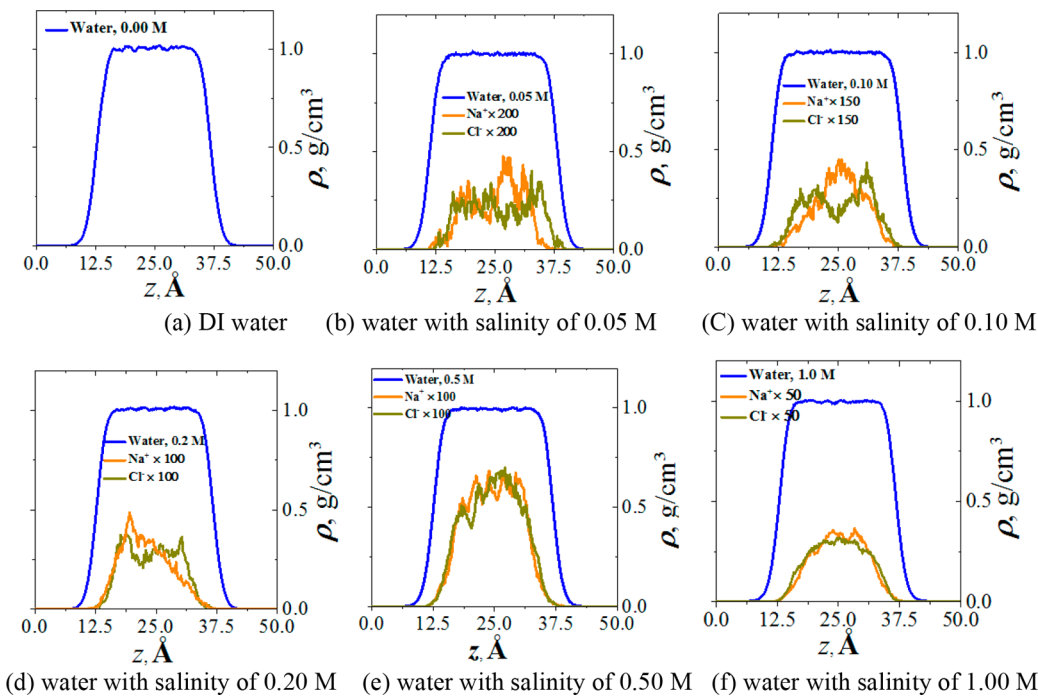


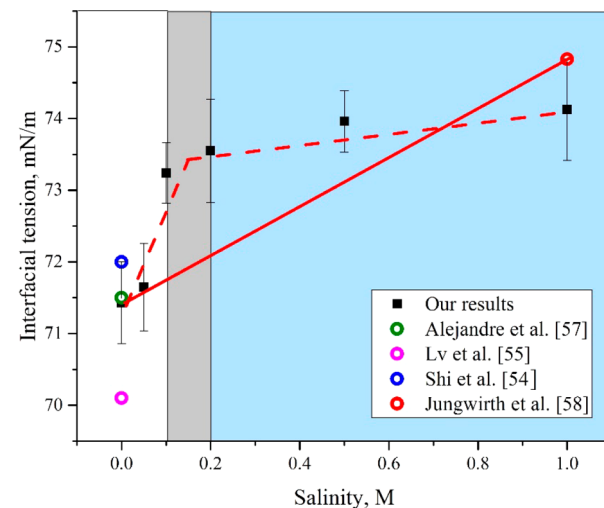
**Figure 3.**  $z$ -density profiles for the various components of the six aqueous NaCl solution systems.

potential energy. (2) The RDFs between water molecules are presented in Figure 2b. It can be observed that  $g(r)$  equals 0 at a short distance, which indicates strong repulsive forces between two water molecules in the short range. The first peak occurs at 2.8 Å with  $g(r)$  arriving around a value of 3, which can be interpreted as indicating that it is 3 times more likely to find two oxygen atoms in different water molecules at this separation. At longer distances,  $g(r)$  between two water molecules approaches a value of 1, indicating there is no long-range order. The RDF profiles of both *n*-decane and water components are in good agreement with previous MD simulations and experimental results, with no shifts for the two main peaks.<sup>45–47</sup>

A series of 5 ns MD simulations of aqueous NaCl solutions at different concentrations (0.00, 0.05, 0.10, 0.20, 0.50, and 1.00 M) were also performed for investigating the salinity effect on the water/vapor interface. The structure of the saltwater/vapor interface was investigated by calculating the mass density profiles along the  $z$  direction perpendicular to the interfacial plane  $xy$ , as shown in Figure 3. The results show that the ion concentration has little effect on the bulk water density, with a stable overall value of around 1.0 g/cm<sup>3</sup>. Besides, although ions move thermodynamically within the water phase, as shown in Figure 6, both sodium and chloride ions are repelled from the water/vapor interface, leaving an almost ion-free interface layer, as shown in the ion density distribution profiles in Figure 3. This phenomenon behaves in accordance with the standard theory of the air/water interface for electrolytes<sup>48</sup> and is reflected experimentally by an increase in the measured surface tension. When the water salinity is lower than 0.20 M, the chloride ions penetrate toward the interface next to the ion-free layer and exhibit a concentration peak, followed by a subsurface depletion. The repulsion of counterions and the subsurface neutrality requirement demonstrates the fact that the sodium cations are dragged by the anions and, consequently, exhibit a subsurface peak.

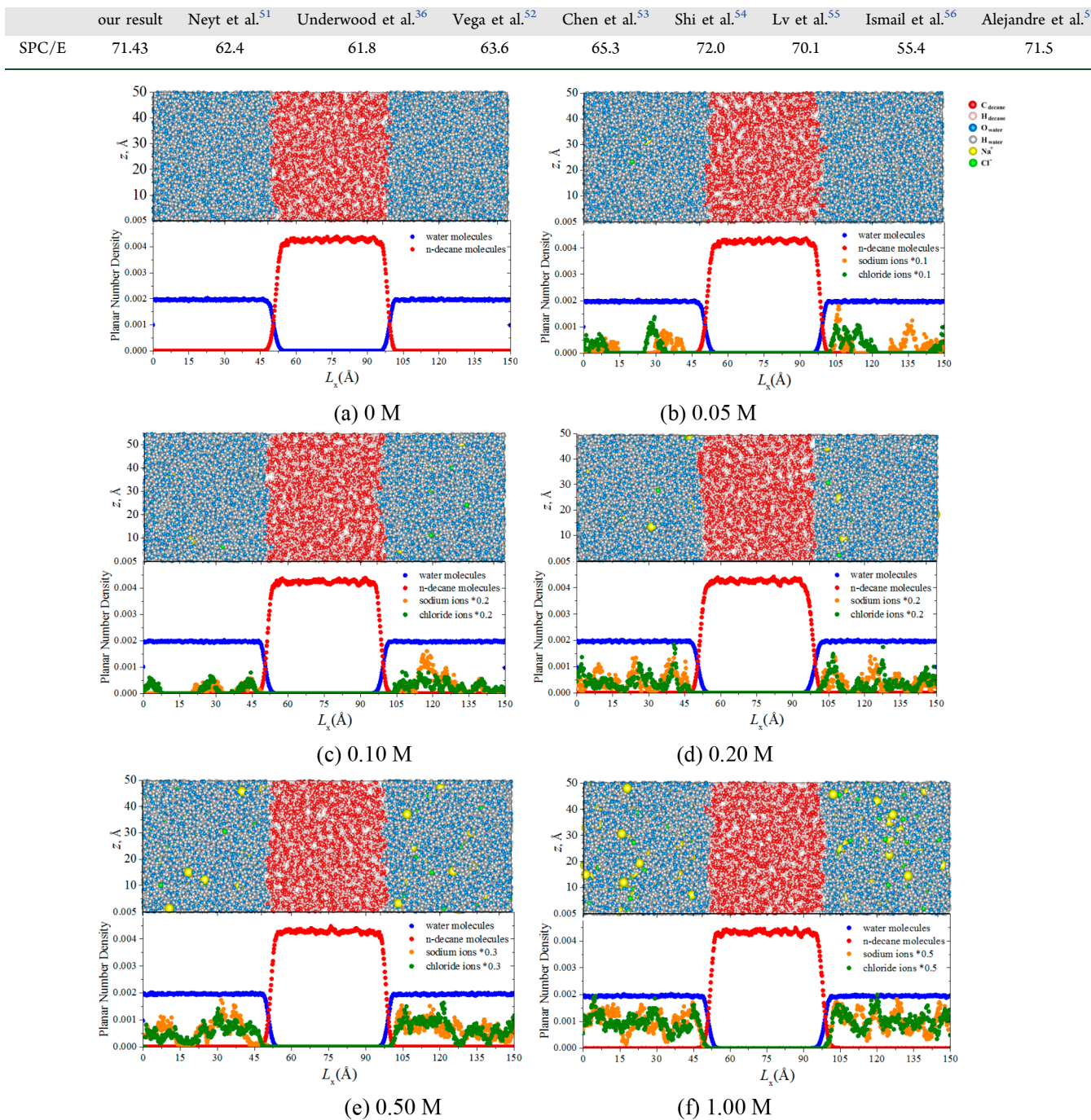
However, this effect becomes weakened when the water salinity is larger than 0.20 M.

To further confirm that an equilibrated system had been obtained in the simulations, the IFT between saltwater and the vapor phase was calculated from the molecular pressure tensor with 1 ns of time averaging, as displayed in Figure 4. The



**Figure 4.** Salinity effect on the IFT of the water/vacuum interface.

“block-averaging” approach, first reported by Flyvbjerg and Petersen,<sup>49</sup> was adopted in this work to determine the property value for a given variable, which has been identified as a simple, relatively robust procedure for estimating statistical uncertainty.<sup>50</sup> The standard error for the IFT was calculated from 10 IFT values using the pressure tensor, for which each value was obtained from a 0.2 ns length of the local pressure distribution data following equilibration. The typical equilibrated *n*-decane/vapor and DI water/vapor IFT values of  $20.54 \pm 1.87$  and  $71.43 \pm 0.57$  mN/m are obtained by averaging the

**Table 1.** SPC/E Water/Vapor IFT from Different MD Simulations (mN/m)**Figure 5.** *n*-Decane/saltwater equilibrated interfaces at different salinities.

last 2 ns of the trajectory with an averaging step of 10 ps. In previous MD simulations, even here conflicting water/vapor IFT values are reported, despite the use of the same SPC/E potential in the simulations, with values varying from 55.4 to 72 mN/m, as summarized in Table 1.

The conflicting values of surface tension for the SPC/E water system can mostly be traced to a variety of numerical issues, resulting from the use of different size-dependent systems, different ensembles (NPT or NVT), different thermostats (Nosé–Hoover or Berendsen), combining different methodologies for determining the electrostatic interactions [e.g., particle–particle particle–mesh (PPPM) and

particle mesh Ewald (PME)], using alternatively the SHAKE or SETTLE algorithm to constrain the water molecule geometry, etc. Our calculated value of 71.43 mN/m using the SPC/E water model at 300 K appears to be in good agreement with the studies of the surface tension of SPC/E water of Alejandre et al.,<sup>57</sup> Shi et al.,<sup>54</sup> Lv et al.,<sup>55</sup> and Jungwirth et al.<sup>58</sup> and also compares well to the experimental value of 71.3–71.6 mN/m, indicating the validity and stability of our calculation setup.

In agreement with experimental measurements, results from the MD simulations shown in Figure 4 indicate that (a) the IFT of the NaCl solutions is greater than that of pure water

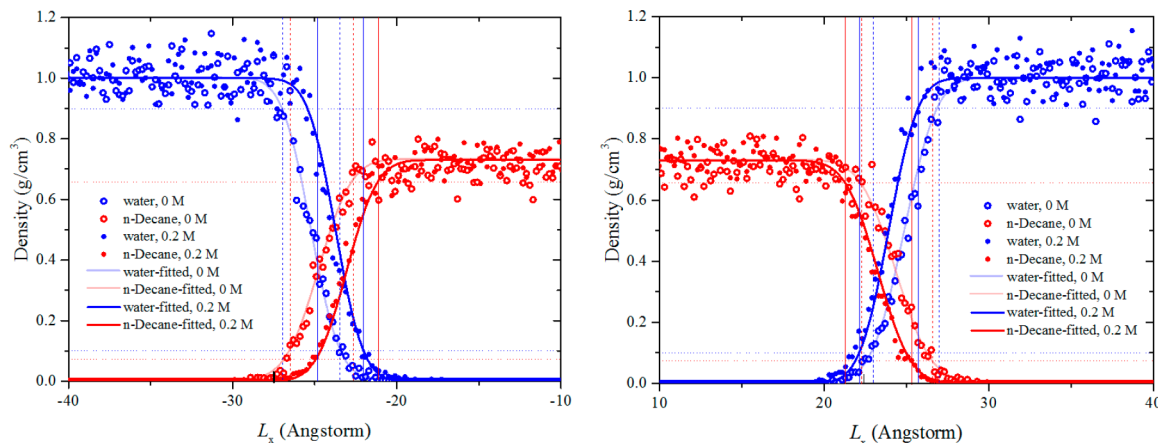


**Figure 6.** Planar (yz) density profiles  $\rho(f_c)$  as a function of the box length  $L_x$  system and the definition of “10–50” interfacial thickness for the saltwater/*n*-decane system.

and (b) increasing the NaCl concentration increases the surface tension of the solution/vapor interface. It may be noted that, when computing the surface tension from the pressure tensor distribution, the increase in saltwater/vapor IFT appears not to be a linear function of the water salinity. With the start of salinity of around 0.10–0.20 M, the rate of increase in the simulated IFT becomes less (although continuously increasing, there is an “inflection point” of IFT at the salt concentration of ~0.20 M). This phenomenon has been mostly neglected in previous experiments/simulations by simply concluding that surface tensions of inorganic electrolyte aqueous solutions were often summarized to be linear functions of the salt concentration. However, these simple linear relationships may not be sufficient to explain observations at the nanoscale, where deviations of water/vapor IFT from the monotonic linear increase exist, e.g., (i) the MD results from Bhatt et al.,<sup>59</sup> (ii) the MD results also using the SPC/E water model by Wang et al.,<sup>60</sup> and (iii) those determined by the differential Köhler analysis (DKA) approach.<sup>61</sup> Using the same MD simulation method and calculation setup, the interface systems between saltwater and the *n*-decane phase were simulated, and the results are reported in the next section.

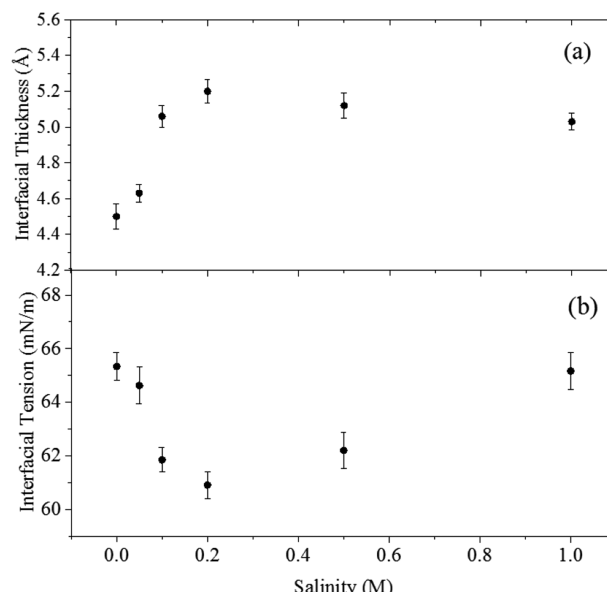
**3.2. Effects of Salinity on Saltwater/*n*-Decane Interfacial Equilibrium.** The salinity effect on the water/*n*-decane interface system is reported in this section at six electrolyte concentrations of 0.00, 0.05, 0.10, 0.20, 0.50, and 1.00 M, respectively.

Figure 5 presents the final equilibrium configuration snapshots of the saltwater/*n*-decane interface system after 5 ns simulations, representing different NaCl concentrations, along with the number density profiles of each system along the *x*-axis direction, perpendicular to the water/*n*-decane interface. It is clear that, in every case, the saltwater/*n*-decane system consists of two phases with two, well-defined interfaces, as deduced from the representation of the water and organic phase molecular density along the direction perpendicular to the interface, representing the immiscibility of saltwater and organic phases. In addition, an almost ion-free layer can also be observed at the saltwater/*n*-decane interface.

To characterize the saltwater/*n*-decane interface thickness, the “10–50” interfacial thickness criterion, derived from the density profiles of both saltwater and *n*-decane phases along the *x*-axis direction in the saltwater/*n*-decane interface system are illustrated in Figure 6 for salt concentrations of 0.00 and

0.20 M. Bulk density values for the water and *n*-decane phases are observed with values around 1.00 and 0.73 g/cm<sup>3</sup>, respectively, with the interface density transition profiles in between.

Figure 7 shows the salinity effect on both the interfacial thickness and IFT for the saltwater/*n*-decane interface systems.



**Figure 7.** (a) “10–50” interfacial thickness and (b) IFT as a function of salinity for the *n*-decane/saltwater interface.

With an increase in the salt concentration from 0 to 1.0 M, the saltwater/*n*-decane interfacial thickness has a maximum value when the salt concentration is 0.2 M, as shown in Figure 7a. Through averaging the IFT fluctuation profile in the period of the last 1 ns with an averaging time step of 10 ps, the corresponding IFT between saltwater and *n*-decane is shown in Figure 7b. The result indicates an opposite trend in the variation of interfacial thickness with an increase of water salinity. A minimum water/*n*-decane IFT value of 61.8 mN/m is predicted at an electrolyte concentration of 0.20 M. The typical calculated DI water/*n*-decane interfacial thickness value of  $4.5 \pm 0.7$  Å and IFT of  $65.33 \pm 0.12$  mN/m are obtained, which are comparable to published experimental and simulation results,<sup>21,30,31</sup> as presented in Table 2.

**Table 2. Interfacial Thickness and IFT between *n*-Decane and DI Water at 300 K for the Water/*n*-Decane System**

	interfacial thickness, $t$ (Å)	IFT, $\gamma$ (mN/m)
our calculated value	$4.5 \pm 0.7$	$65.33 \pm 0.12$
experimental result <sup>31</sup>	$4.6 \pm 0.2$	51.72
MD simulation value <sup>21</sup>	6.5	58.32
MD simulation value <sup>30</sup>	3.90	$66 \pm 4$

To identify the mechanism by which monovalent ions affect the saltwater/oil interface, the RDFs for each component in the saltwater/*n*-decane binary systems are analyzed in Figure 8. It can be observed from Figure 8a that the presence of ions has little effect on the interactions between *n*-decane molecules in the oil phase. This is due to the insolubility of ions in the decane phase, which is indicated in Figure 8b, where no dominant peak appeared in the RDF profile and the ions

remain in the water phase. The solubility of the electrolyte ions in the water phase explains the first peak in the RDF profile between ions and water molecules, as shown in Figure 8c, which represents the hydration structure of the ions. The effect of salinity on the molecular structure of the water phase is displayed in Figure 8d. It can be seen that the second peak in the water molecule pair correlation function gradually disappears with an increasing electrolyte concentration, indicating that the presence of ions forces water molecules to occupy interstitial positions, and thus, no well-defined second hydration shell is found around a central water molecule. For the interaction between aqueous  $\text{Na}^+$  and  $\text{Cl}^-$  ions, shown in Figure 8e, the first peaks at around 3 Å show the presence of contact ion pairs in the solution. The second peak, at around 5.2 Å, corresponds to the presence of solvent-separated ion pairs in NaCl solutions. With the increase of the electrolyte concentration, the probability of contact ion pair

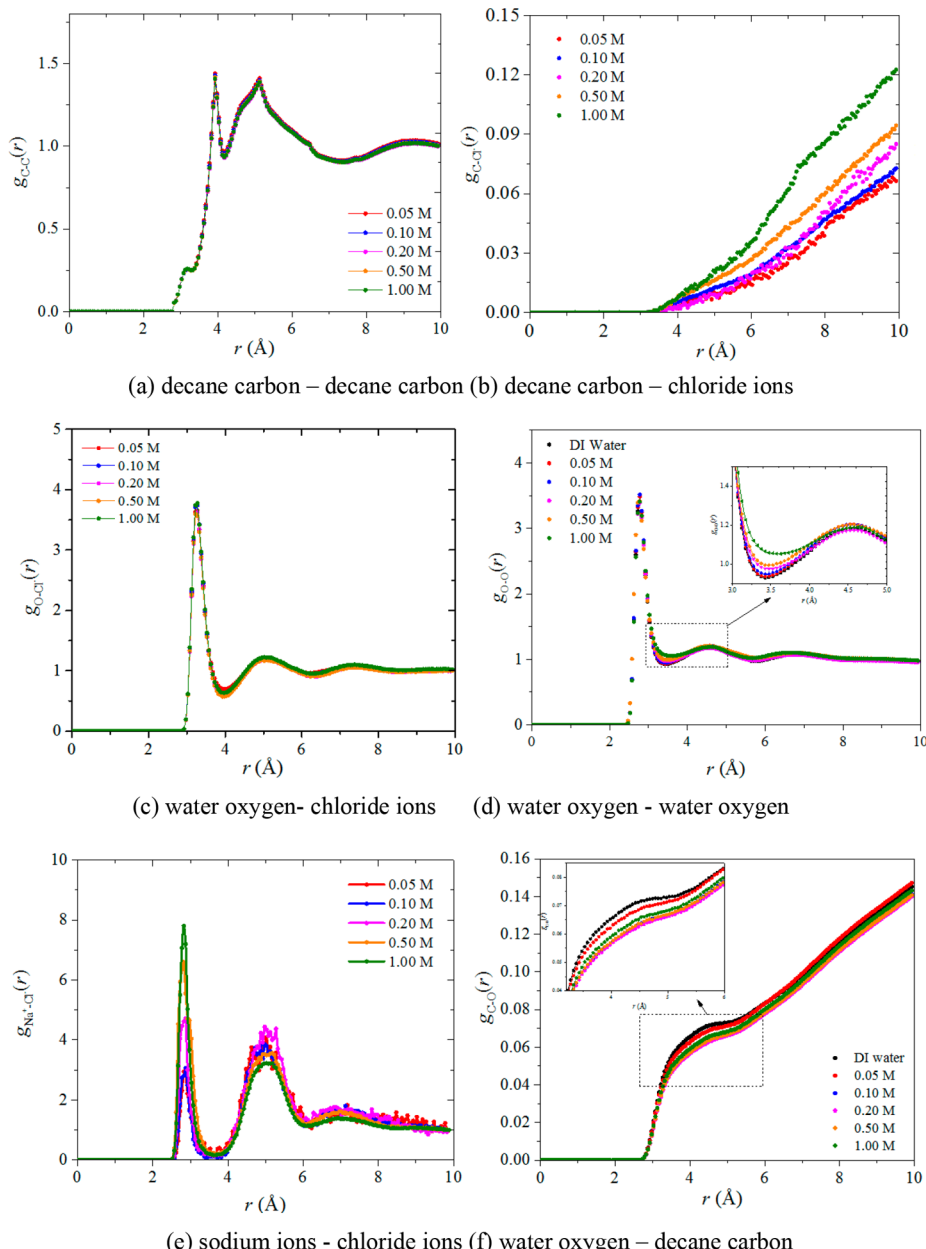


**Figure 8.** RDFs for the saltwater/*n*-decane interface system.

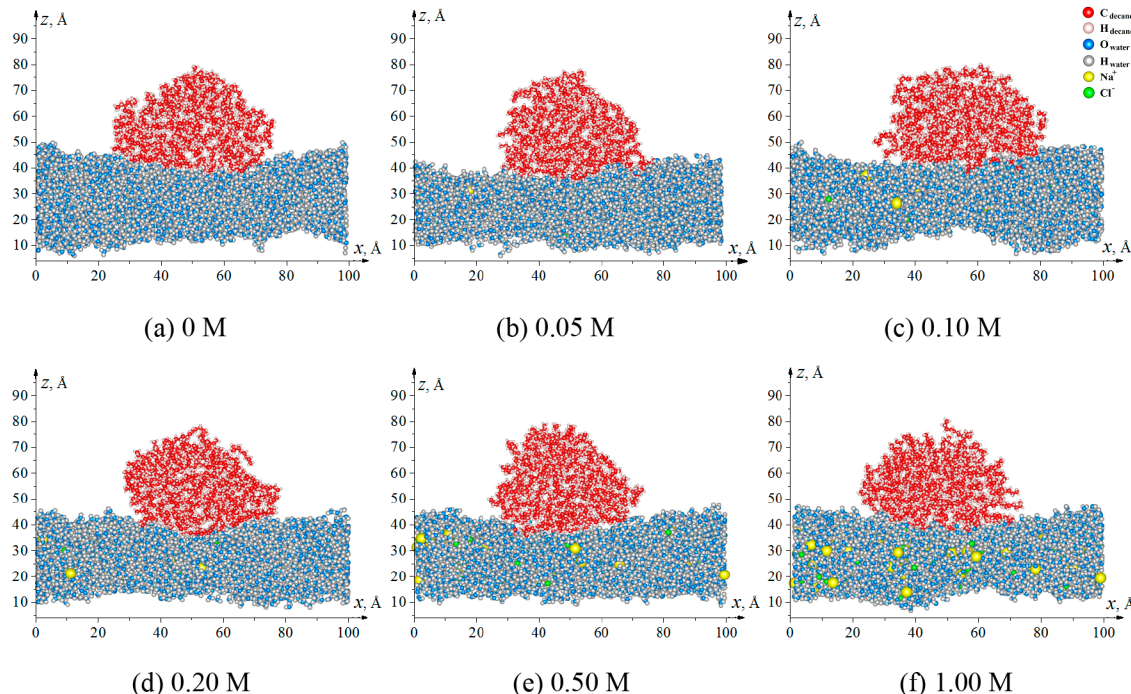


**Figure 9.** Series of snapshots of decane–salinity water–vacuum three-phase system.

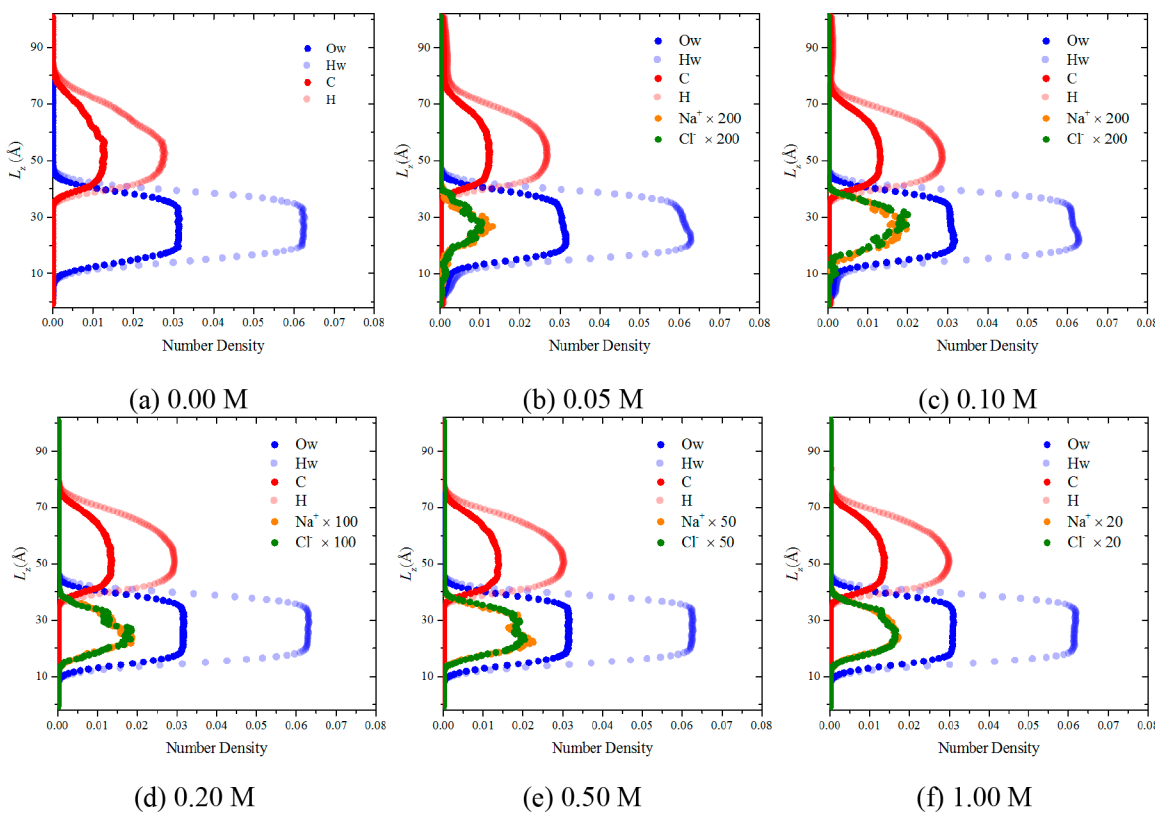


**Figure 10.** Number density along the  $z$ -axis direction of the decane–salinity water–vacuum three-phase system.

formation increases and that of solvent-separated ion pair formation decreases for the solution. The effect of salinity on the interaction between water and the decane phase can be observed from the RDF profile between water and decane molecules, as shown in Figure 8f. No significant peaks can be observed here but only a continuously increasing trend, which

is consistent with the immiscibility of water and *n*-decane phases. However, an apparent curvature change is manifested along the increasing RDF profile between 3 and 6 Å, indicating adsorption interactions between water and the *n*-decane phase at the saltwater/*n*-decane interface. It can be seen that the weakest adsorption between water and *n*-decane occurs when

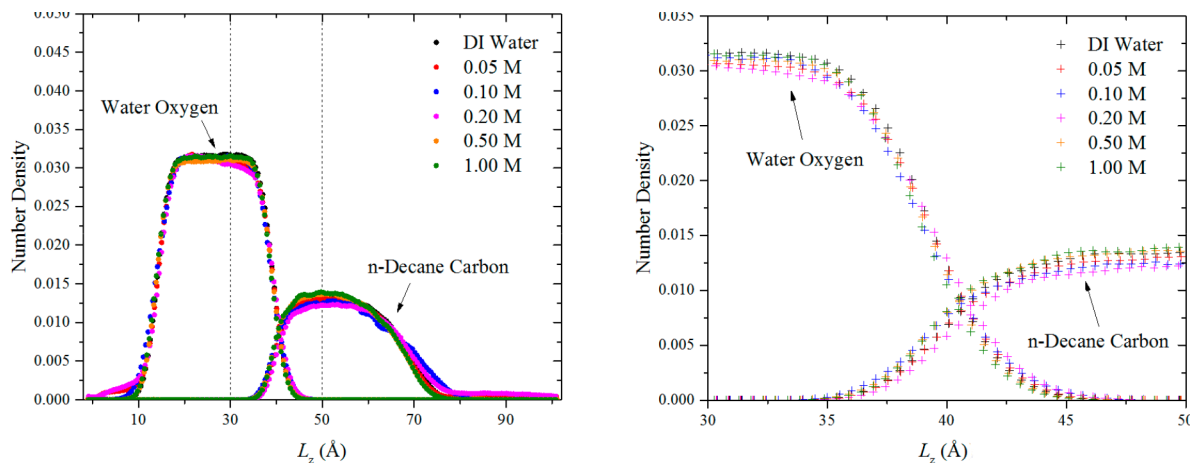


**Figure 11.**  $z$ -density distribution of water oxygen and *n*-decane carbon at different electrolyte concentrations.

the electrolyte concentration is 0.20 M, demonstrating the loosest of the interface structures. This phenomenon also corresponds to the calculated equilibrium “10–50” interfacial thickness variations with water salinity, which is caused by the combination of attractive interactions between water and ions and repulsive interactions between *n*-decane and ions, which controls the IFT between saltwater and the *n*-decane phase.

**3.3. Effect of Salinity on the *n*-Decane/Water/Vapor Three-Phase System.** MD simulation results concerning the effect of salinity on the *n*-decane/water/vapor three-phase system are presented in this section. As the initial simulation configurations, outlined in section 2.1, the rectangular *n*-decane phase and water slab systems were created with a minimum distance of 4 Å. The final snapshots of an *n*-decane/water/vapor interface unit cell with different salinities, after 5.0 ns of simulation time, are shown in Figure 9. It can be observed that the *n*-decane molecules have relaxed to form a two-dimensional (2D) cylindrical shape, approaching a lens on the water slab surface caused by attractive interactions as a result of the van der Waals and Columbic forces between the constituent molecules. After the *n*-decane droplet is spread on the water surface, it finally forms an elliptically shaped droplet on the water slab surface. After equilibration, the *n*-decane droplet keeps its shape apart from the effect of thermal fluctuations, as shown in Figure 9.

During the MD simulation, the three-phase system remains continuous in the  $z$ -axis direction, as shown in Figure 10. To investigate the detail of the shape of the *n*-decane/saltwater/vapor three-phase system, the Gibbs dividing surface was calculated from the density profiles of *n*-decane and water phases along the  $z$ -axis direction, as presented in Figure 11. The contact angles were thus obtained from the directions of the upper and lower sides of the *n*-decane droplet,<sup>33</sup> which were fitted as a sphere with a least squares method. To quantify the fluctuation effect in the error analysis, using the block-averaging approach, density distributions of each component were calculated over 0.2 ns time intervals for the last 2 ns of simulation of the equilibrated trajectory. In this step, a total of 10 density distributions were obtained, resulting in 10 values of the contact angle. Further, the equilibrium density distribution and contact angle value were averaged over the last 2 ns. The variance between the averages for these 10 values is presented as the uncertainty. The contact angle variation with water salinity for the three-phase system is presented in Figure 12a, which indicates a maximum contact angle value of 64.88° at a

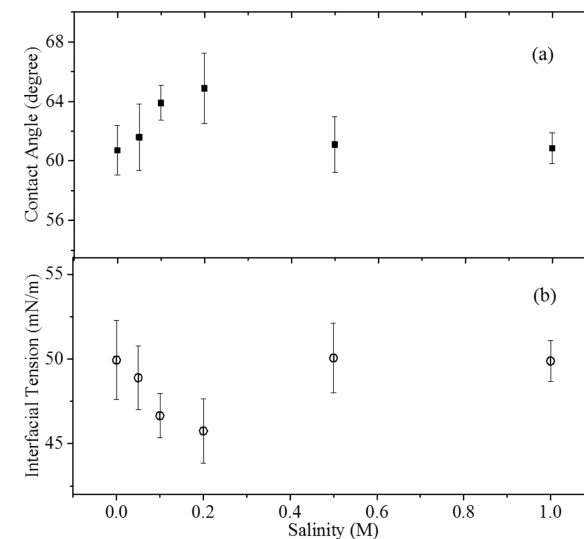


**Figure 12.** (a) “10–50” interfacial thickness and (b) surface tension as a function of salinity for the *n*-decane/water/vapor three-phase interface system.

salinity of 0.20 M. The corresponding IFT variations between saltwater and *n*-decane phases shown in Figure 12b have an opposite trend to the contact angle variations. An optimal minimum water/*n*-decane IFT occurs at a salt concentration of 0.20 M, and such a minimum is considered optimal for EOR. Qualitatively, such a trend is consistent with some experimental studies at the macroscale.<sup>40</sup>

The RDF profiles for the saltwater/*n*-decane/vapor system are shown in Figure 13. The salinity effects on the water–water and water–ion interaction profiles of the saltwater/*n*-decane/vapor three-phase interface system are similar to that for the saltwater/*n*-decane interface system, as shown in panels a and b of Figure 13. Both the sodium and chloride ion hydration effects can also be observed, as presented in panels c and d of Figure 13. Figure 13e characterizes the sodium ion and *n*-decane molecule interactions as a function of the electrolyte concentration. No dominant peaks are observed in the RDF profile between ions and molecules of *n*-decane in the organic phase, which indicates that all ions remain in the water slab phase instead of transferring to the *n*-decane phase. In combination of the hydration effect of the ions and the repulsion effect between ions and the oil phase, the overall

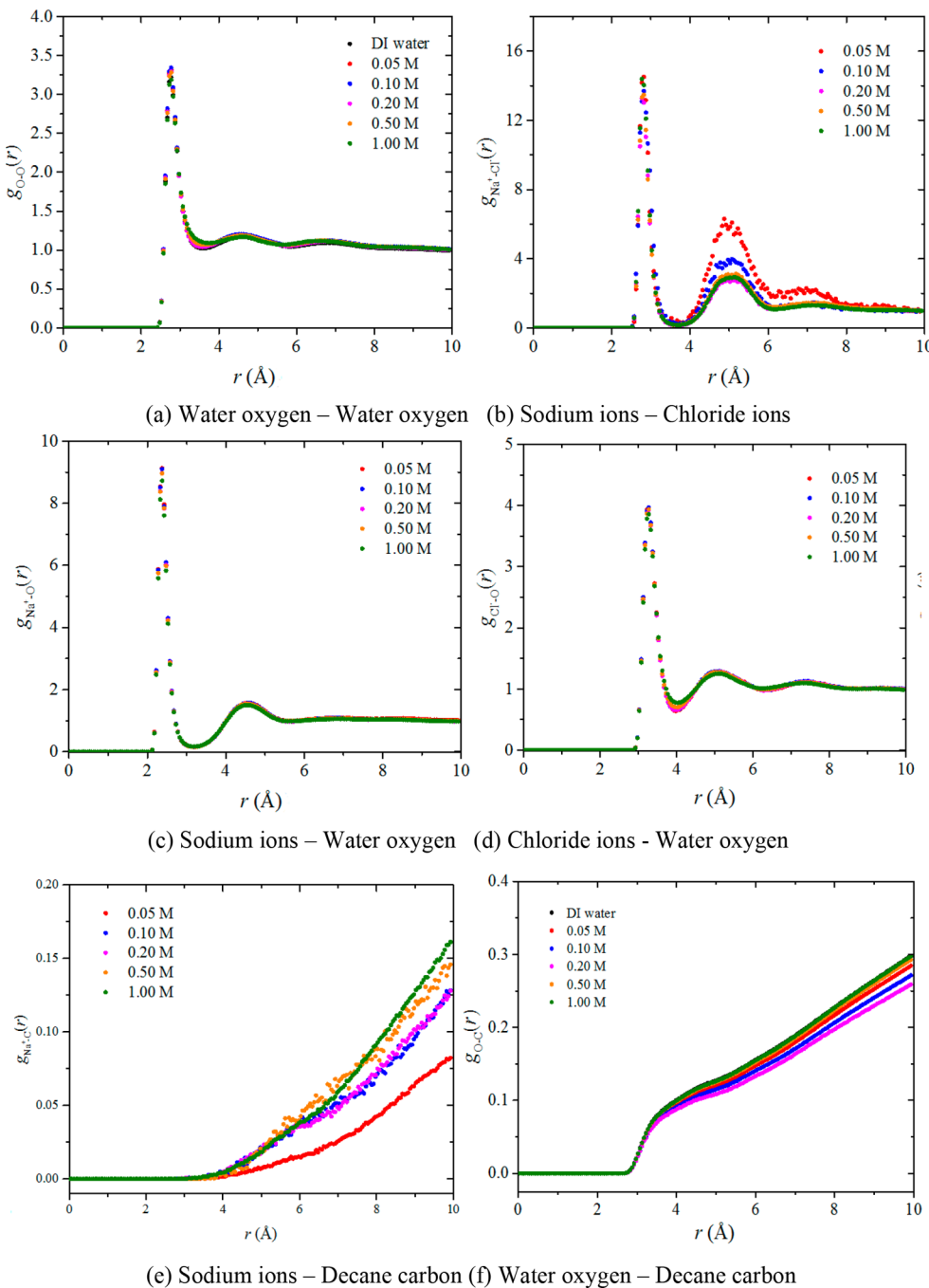


**Figure 13.** RDF for the water/*n*-decane/vapor system with different salinities.

water–oil interaction is shown in Figure 13f, which suggests that the loosest interface structure between water and *n*-decane phases is manifested when the electrolyte concentration is around 0.20 M. Qualitatively, such trends are consistent with experimental studies at the macroscale.<sup>62</sup>

#### 4. CONCLUSION

As part of increasing our understanding of the mechanism that underpins experimental observations of a benefit in injecting low-salinity water for EOR, otherwise known as “the salinity effect”, MD simulations have been performed to model interfaces between water and oil. The results of these simulations can be summarized as follows: (1) The IFT of the water/vapor, *n*-decane/vapor, and water/*n*-decane inter-

faces were calculated from the pressure tensor distribution after the simulations reached an equilibrated state, with values of 71.43, 20.54, and 65.33 mN/m, respectively. The calculated IFT values show good agreement with previous experimental and simulation results. (2) An optimal water salinity value is observed around 0.20 M for the equilibrated water/oil interface system, which has the maximum interfacial thickness between water and the oil phase, corresponding to the minimum water/oil IFT value. (3) An optimal water salinity condition at around 0.20 M is also predicted by investigating the equilibrium water/oil/vapor interface system with the maximum contact angle between water and the oil phase, contributing to the minimum saltwater/oil IFT value, which is a condition beneficial for EOR.

The presented work indicates that the molecular level insight into saltwater/oil/vapor interactions and interfacial equilibrium properties offers hitherto unaccessed resolution for EOR applications using the atomistic MD simulation method. Future work will investigate the saltwater/oil/vapor interactions in a mineral nanoslit pore. Both the salinity effect and mineral surface substrate on the oil wettability and recovery factor during EOR will be modeled.

## AUTHOR INFORMATION

### Corresponding Author

\*E-mail: [d.wen@leeds.ac.uk](mailto:d.wen@leeds.ac.uk) and [d.wen@buaa.edu.cn](mailto:d.wen@buaa.edu.cn).

### ORCID®

Jin Zhao: [0000-0002-8714-7798](https://orcid.org/0000-0002-8714-7798)

Dongsheng Wen: [0000-0003-3492-7982](https://orcid.org/0000-0003-3492-7982)

### Notes

The authors declare no competing financial interest.

## ACKNOWLEDGMENTS

This work was supported by the European Research Council Consolidator Grant (Grant 648375), the China Scholarship Council (201506450021) and the 111 project (B18002).

## REFERENCES

- (1) Muggeridge, A.; Cockin, A.; Webb, K.; Frampton, H.; Collins, I.; Moulds, T.; Salino, P. Recovery rates, enhanced oil recovery and technological limits. *Philos. Trans. R. Soc., A* **2014**, *372*, 20120320.
- (2) Morrow, N.; Buckley, J. Improved oil recovery by low-salinity water flooding. *JPT, J. Pet. Technol.* **2011**, *63* (05), 106–112.
- (3) Jadhunandan, P. P. Effects of brine composition, crude oil, and aging conditions on wettability and oil recovery. Doctoral Dissertation, Department of Petroleum and Natural Gas Engineering, New Mexico Institute of Mining and Technology, Socorro, NM, 1990.
- (4) Austad, T.; Shariatpanahi, S. F.; Strand, S.; Black, C. J. J.; Webb, K. J. Conditions for a low-salinity enhanced oil recovery (EOR) effect in carbonate oil reservoirs. *Energy Fuels* **2012**, *26* (1), 569–575.
- (5) Sheng, J. J. Critical review of low-salinity waterflooding. *J. Pet. Sci. Eng.* **2014**, *120*, 216–224.
- (6) Nasralla, R. A.; Nasr-El-Din, H. A. Double-layer expansion: Is it a primary mechanism of improved oil recovery by low-salinity waterflooding? *SPE Res. Eval. Eng.* **2014**, *17* (01), 49–59.
- (7) Zhang, H.; Dong, M.; Zhao, S. Which one is more important in chemical flooding for enhanced court heavy oil recovery, lowering interfacial tension or reducing water mobility? *Energy Fuels* **2010**, *24* (3), 1829–1836.
- (8) Underwood, T.; Erastova, V.; Cubillas, P.; Greenwell, H. C. Molecular dynamic simulations of montmorillonite–organic interactions under varying salinity: An insight into enhanced oil recovery. *J. Phys. Chem. C* **2015**, *119* (13), 7282–7294.
- (9) Nicolini, J. V.; Ferraz, H. C.; Borges, C. P. Effect of seawater ionic composition modified by nanofiltration on enhanced oil recovery in Berea sandstone. *Fuel* **2017**, *203*, 222–232.
- (10) Al-Khafaji, A.; Neville, A.; Wilson, M.; Wen, D. Effect of low salinity on the oil desorption efficiency from calcite and silica surfaces. *Energy & Fuels* **2017**, *31* (11), 11892–11901.
- (11) Aveyard, R.; Saleem, S. M. Interfacial tensions at alkane-aqueous electrolyte interfaces. *J. Chem. Soc., Faraday Trans. 1* **1976**, *72*, 1609–1617.
- (12) Ikeda, N.; Aratono, M.; Motomura, K. Thermodynamic study on the adsorption of sodium chloride at the water/hexane interface. *J. Colloid Interface Sci.* **1992**, *149* (1), 208–215.
- (13) Badakshan, A.; Bakes, P. The influence of temperature and surfactant concentration on interfacial tension of saline water and hydrocarbon systems in relation to enhanced oil recovery by chemical flooding. *Soc. Pet. Eng.* **1990**.
- (14) Cai, B.-Y.; Yang, J.-T.; Guo, T.-M. Interfacial tension of hydrocarbon + water/brine systems under high pressure. *J. Chem. Eng. Data* **1996**, *41* (3), 493–496.
- (15) Serrano-Saldaña, E.; Domínguez-Ortiz, A.; Pérez-Aguilar, H.; Kornhauser-Strauss, I.; Rojas-González, F. Wettability of solid/brine/n-dodecane systems: Experimental study of the effects of ionic strength and surfactant concentration. *Colloids Surf., A* **2004**, *241* (1–3), 343–349.
- (16) Alotaibi, M. B.; Nasr-El-Din, H. A. Salinity of injection water and its impact on oil recovery. *Proceedings of the EUROPEC/EAGE Conference and Exhibition*; Amsterdam, Netherlands, June 8–11, 2009; DOI: [10.2118/121569-MS](https://doi.org/10.2118/121569-MS).
- (17) Khusainova, A.; Nielsen, S. M.; Pedersen, H. H.; Woodley, J. M.; Shapiro, A. Study of wettability of calcite surfaces using oil–brine–enzyme systems for enhanced oil recovery applications. *J. Pet. Sci. Eng.* **2015**, *127*, 53–64.
- (18) Fenter, P.; Kerisit, S.; Raiteri, P.; Gale, J. D. Is the calcite–water interface understood? Direct comparisons of molecular dynamics simulations with specular X-ray reflectivity data. *J. Phys. Chem. C* **2013**, *117* (10), 5028–5042.
- (19) Zhang, H.; Nikolov, A.; Wasan, D. Enhanced oil recovery (EOR) using nanoparticle dispersions: Underlying mechanism and imbibition experiments. *Energy Fuels* **2014**, *28* (S), 3002–3009.
- (20) Turgman-Cohen, S.; Araque, J. C.; Hoek, E. M. V.; Escobedo, F. A. Molecular dynamics of equilibrium and pressure-driven transport properties of water through LTA-type zeolites. *Langmuir* **2013**, *29* (40), 12389–12399.
- (21) Chen, X.; Munjiza, A.; Zhang, K.; Wen, D. Molecular dynamics simulation of heat transfer from a gold nanoparticle to a water pool. *J. Phys. Chem. C* **2014**, *118* (2), 1285–1293.
- (22) Jorgensen, W. L.; Tirado-Rives, J. The OPLS [optimized potentials for liquid simulations] potential functions for proteins, energy minimizations for crystals of cyclic peptides and crambin. *J. Am. Chem. Soc.* **1988**, *110* (6), 1657–1666.
- (23) Bankura, A.; Carnevale, V.; Klein, M. L. Hydration structure of salt solutions from ab initio molecular dynamics. *J. Chem. Phys.* **2013**, *138* (1), 014501.
- (24) Jungwirth, P.; Tobias, D. J. Specific ion effects at the air/water interface. *Chem. Rev.* **2006**, *106* (4), 1259–1281.
- (25) D'Auria, R.; Tobias, D. J. Relation between Surface Tension and Ion Adsorption at the Air–Water Interface: A Molecular Dynamics Simulation Study. *J. Phys. Chem. A* **2009**, *113* (26), 7286–7293.
- (26) Brown, M. A.; D'Auria, R.; Kuo, I.-F. W.; Krisch, M. J.; Starr, D. E.; Bluhm, H.; Tobias, D. J.; Hemminger, J. C. Ion spatial distributions at the liquid–vapor interface of aqueous potassium fluoride solutions. *Phys. Chem. Chem. Phys.* **2008**, *10* (32), 4778–4784.
- (27) Sun, L.; Li, X.; Hede, T.; Tu, Y.; Leck, C.; Ågren, H. Molecular dynamics simulations of the surface tension and structure of salt solutions and clusters. *J. Phys. Chem. B* **2012**, *116* (10), 3198–3204.
- (28) Van Buuren, A. R.; Marrink, S. J.; Berendsen, H. J. A molecular dynamics study of the decane/water interface. *J. Phys. Chem.* **1993**, *97* (36), 9206–9212.
- (29) Zeppieri, S.; Rodríguez, J.; López de Ramos, A. L. Interfacial tension of alkane + water systems. *J. Chem. Eng. Data* **2001**, *46* (S), 1086–1088.
- (30) Jang, S. S.; Lin, S. T.; Maiti, P. K.; Blanco, M.; Goddard, W. A.; Shuler, P.; Tang, Y. Molecular dynamics study of a surfactant-mediated decane–water interface: Effect of molecular architecture of alkyl benzene sulfonate. *J. Phys. Chem. B* **2004**, *108* (32), 12130–12140.
- (31) Mitrinović, D. M.; Tikhonov, A. M.; Li, M.; Huang, Z.; Schlossman, M. L. Noncapillary-wave structure at the water-alkane interface. *Phys. Rev. Lett.* **2000**, *85* (3), 582.
- (32) Kunieda, M.; Liang, Y.; Fukunaka, Y.; Matsuoka, T.; Takamura, K.; Loahardjo, N.; Winoto, W.; Morrow, N. R. Spreading of Multi-component Oils on Water. *Energy Fuels* **2012**, *26* (5), 2736–2741.

- (33) Kunieda, M. Molecular Dynamics Study of Oil–Water Interfacial Equilibrium in Petroleum Engineering. Ph.D. Dissertation, Kyoto University, Kyoto, Japan, 2012.
- (34) Zhang, C.; Carloni, P. Salt effects on water/hydrophobic liquid interfaces: A molecular dynamics study. *J. Phys.: Condens. Matter* **2012**, *24* (12), 124109.
- (35) Martínez, L.; Andrade, R.; Birgin, E. G.; Martínez, J. M. PACKMOL: A package for building initial configurations for molecular dynamics simulations. *J. Comput. Chem.* **2009**, *30* (13), 2157–2164.
- (36) Dang, L. X.; Smith, D. E. Molecular dynamics simulations of aqueous ionic clusters using polarizable water. *J. Chem. Phys.* **1993**, *99* (9), 6950–6956.
- (37) Underwood, T. R.; Greenwell, H. C. The Water–Alkane Interface at Various NaCl Salt Concentrations: A Molecular Dynamics Study of the Readily Available Force Fields. *Sci. Rep.* **2018**, *8* (1), 352.
- (38) Mohammed, S.; Mansoori, G. A. Effect of CO<sub>2</sub> on the Interfacial and Transport Properties of Water/Binary and Asphaltenic Oils: Insights from Molecular Dynamics. *Energy Fuels* **2018**, *32* (4), 5409–5417.
- (39) Jian, C.; Liu, Q.; Zeng, H.; Tang, T. A Molecular Dynamics Study of the Effect of Asphaltenes on Toluene/Water Interfacial Tension: Surfactant or Solute? *Energy Fuels* **2018**, *32* (3), 3225–3231.
- (40) Smith, W.; Yong, C. W.; Rodger, P. M. DL\_POLY: Application to molecular simulation. *Mol. Simul.* **2002**, *28* (5), 385–471.
- (41) Ono, S.; Kondo, S. Molecular theory of surface tension in liquids. In *Structure of Liquids/Struktur der Flüssigkeiten*; Flügge, S., Ed.; Springer: Berlin, Germany, 1960; Vol. 3/10, pp 134–280, DOI: [10.1007/978-3-642-45947-4\\_2](https://doi.org/10.1007/978-3-642-45947-4_2).
- (42) Hill, T. L. *An Introduction to Statistical Thermodynamics*; Courier Corporation: New York, 1960.
- (43) Alejandre, J.; Tildesley, D. J.; Chapela, G. A. Fluid phase equilibria using molecular dynamics: The surface tension of chlorine and hexane. *Mol. Phys.* **1995**, *85* (3), 651–663.
- (44) Senapati, S.; Berkowitz, M. L. Computer simulation study of the interface width of the liquid/liquid interface. *Phys. Rev. Lett.* **2001**, *87* (17), 176101.
- (45) Ryckaert, J. P.; Bellemans, A. Molecular dynamics of liquid alkanes. *Faraday Discuss. Chem. Soc.* **1978**, *66*, 95–106.
- (46) Spyrou, M. The Diffusion Coefficient of Water: A Neutron Scattering Study Using Molecular Dynamics Simulations. Master's Dissertation, Department of Physics, University of Surrey, Guildford, U.K., 2009.
- (47) Sorenson, J. M.; Hura, G.; Glaeser, R. M.; Head-Gordon, T. What can X-ray scattering tell us about the radial distribution functions of water? *J. Chem. Phys.* **2000**, *113* (20), 9149–9161.
- (48) Onsager, L.; Samaras, N. N. The surface tension of Debye-Hückel electrolytes. *J. Chem. Phys.* **1934**, *2* (8), 528–536.
- (49) Flyvbjerg, H.; Petersen, H. G. Error estimates on averages of correlated data. *J. Chem. Phys.* **1989**, *91*, 461–466.
- (50) Grossfield, A.; Zuckerman, D. M. Quantifying uncertainty and sampling quality in biomolecular simulations. *Annual Reports in Computational Chemistry*; Elsevier: Amsterdam, Netherlands, 2009; Vol. 5, Chapter 2, pp 23–48, DOI: [10.1016/S1574-1400\(09\)00502-7](https://doi.org/10.1016/S1574-1400(09)00502-7).
- (51) Neyt, J.; Wender, A.; Lachet, V.; Ghoufi, A.; Malfreyt, P. Prediction of the concentration dependence of the surface tension and density of salt solutions: Atomistic simulations using drude oscillator polarizable and nonpolarizable models. *Phys. Chem. Chem. Phys.* **2013**, *15*, 11679–11690.
- (52) Vega, C.; de Miguel, E. Surface tension of the most popular models of water by using the test-area simulation method. *J. Chem. Phys.* **2007**, *126*, 154707.
- (53) Chen, F.; Smith, P. E. Simulated surface tensions of common water models. *J. Chem. Phys.* **2007**, *126*, 221101.
- (54) Shi, B.; Sinha, S.; Dhir, V. K. Molecular dynamics simulation of the density and surface tension of water by particle–particle particle-mesh method. *J. Chem. Phys.* **2006**, *124*, 204715.
- (55) Lü, Y. J.; Wei, B. Second inflection point of water surface tension. *Appl. Phys. Lett.* **2006**, *89*, 164106.
- (56) Ismail, A. E.; Grest, G. S.; Stevens, M. J. Capillary waves at the liquid–vapor interface and the surface tension of water. *J. Chem. Phys.* **2006**, *125*, 014702.
- (57) Alejandre, J.; Tildesley, D. J.; Chapela, G. A. Molecular dynamics simulation of the orthobaric densities and surface tension of water. *J. Chem. Phys.* **1995**, *102*, 4574–4583.
- (58) Jungwirth, P.; Tobias, D. J. Molecular structure of salt solutions: A new view of the interface with implications for heterogeneous atmospheric chemistry. *J. Phys. Chem. B* **2001**, *105*, 10468–10472.
- (59) Bhatt, D.; Chee, R.; Newman, J.; Radke, C. J. Molecular simulation of the surface tension of simple aqueous electrolytes and the Gibbs adsorption equation. *Curr. Opin. Colloid Interface Sci.* **2004**, *9* (1–2), 145–148.
- (60) Wang, X.; Chen, C.; Binder, K.; Kuhn, U.; Pöschl, U.; Su, H.; Cheng, Y. F. Molecular Dynamics Simulation of the Surface Tension of Aqueous Sodium Chloride: From Dilute to Highly Supersaturated Solutions and Molten Salt. *Atmos. Chem. Phys. Discuss.* **2017**, 1–18.
- (61) Cheng, Y.; Su, H.; Koop, T.; Mikhailov, E.; Pöschl, U. Size dependence of phase transitions in aerosol nanoparticles. *Nat. Commun.* **2015**, *6*, 5923.
- (62) Al-Khafaji, A.; Neville, A.; Wilson, M.; Wen, D. Effect of Low Salinity on the Oil Desorption Efficiency from Calcite and Silica Surfaces. *Energy Fuels* **2017**, *31* (11), 11892–11901.